Aalto University
School of Science

Master's programme in Mathematics and Operations research

Automated optimisation workflow for radiotherapy using dose mimicking from deep learning predicted dose

Saku Myllymäki

Master's Thesis
2024

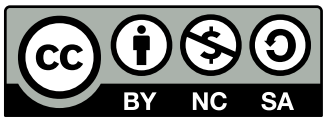

Aalto University
School of Science

Author Saku Myllymäki

Title Automated optimisation workflow for radiotherapy using dose mimicking from deep learning predicted dose

Degree programme Mathematics and Operations research

Major Mathematics

Supervisor Prof. Fabricio Oliveira

Advisor Gregory Bolard, M.Sc.

Collaborative partner MVision AI

Date May 27, 2024 **Number of pages** 43 **Language** English

Abstract

Intensity modulated radiotherapy (IMRT) and volumetric modulated arc therapy (VMAT) are widespread optimisation frameworks used in treatment plan generation for cancer patients today. Practitioners commonly spend a significant amount of time balancing optimisation objectives to produce clinically acceptable treatment plans. Recent work has proved machine learning predicted dose distributions used in conjunction with dose mimicking or structure objectives derived from the predicted dose to be able to produce high quality treatment plans.

In this thesis, the aim was to use MVision's deep learning predicted dose distributions and evaluate different optimisation strategies for producing dose distributions similar in quality. Pure dose mimicking approaches, an approach using dose derived structure objectives in addition to hybrid dose mimicking and structure objective approaches were explored.

For the experiments, MatRad, an open source radiotherapy treatment planning toolkit was used. The toolkit provides a pencil beam dose influence matrix calculation algorithm and an interior point method optimiser package, which were used for dose optimisation. Voxel mimicking approaches were generally not able to mimic the predicted dose distributions and the optimisation dose distributions were of significantly lower quality. No optimisation method was able to consistently reproduce the quality of the predicted dose, but the structure based objectives showed most potential.

Keywords Dose mimicking, deep learning dose prediction, voxel mimicking, IMRT, VMAT

Aalto-yliopisto
Perustieteiden
korkeakoulu

Tekijä Saku Myllymäki

Työn nimi Syväoppimisella ennustetun annosjakauman jäljittely sädetysterapian annosoptimoinnissa

Koulutusohjelma Matematiikka ja Operaatiotutkimus

Pääaine Matematiikka

Työn valvoja Prof. Fabricio Oliveira

Työn ohjaaja DI Gregory Bolard

Yhteistyötaho MVision AI

Päivämäärä 27.5.2024 **Sivumäärä** 43 **Kieli** englanti

Tiivistelmä

Intensiteettimoduloitu sädehoito sekä kaarihoitotekniikka ovat nykyisin laajassa käytössä olevia optimointimenetelmiä syöpäpotilaiden sädehoidon suunnittelussa. Syöpälääkärit käyttävät tyypillisesti huomattavan määrän aikaa optimointitavoitteiden luomiseen sekä tasapainottamiseen laadukkaan annosjakauman tuottavan sädehoitosuunnitelman luomiseksi. Viimeaikainen tutkimus on osoittanut, että koneoppimista hyödyntävien annosennusteiden jäljittely optimoimalla voi tuottaa laadukkaita annoksia.

Tässä diplomityössä tarkoituksena oli hyödyntää MVisionin syväoppimispohjaisia annosennusteita ja arvioida erilaisten optimointistrategioiden kykyä tuottaa yhtä laadukkaita annosjakaumia annosennusteen pohjalta. Tutkimuksen kohteena oli kaksi eri pelkästään annosta jäljittelevää menetelmää, annosennusteen pohjalta annos-tilavuus -tavoitteita luova menetelmä sekä kaksi hybridimenetelmää.

Kokeissa oli käytössä avoimen lähdekoodin sädehoitosuunnittelukirjasto MatRad. Kirjasto tarjoaa intensiteettimodulointiin soveltuvan kernelpohjaisen pencil-beam -algoritmin ja sisäpistemenetelmää käyttävän optimoijan, joita käytettiin annosoptimointiin. Annosta jäljittelevät menetelmät eivät kyenneet jäljittelemään annosennustetta eikä tuottamaan laadukkaita annoksia kaikissa tapauksissa. Yksikään optimointimenetelmä ei tuottanut johdonmukaisesti muita menetelmiä parempia tuloksia, mutta annos-tilavuus -tavoitteet automaattisesti luova menetelmä vaikuttaa lupaavimmalta.

Avainsanat Annosjäljittely, annosennuste, intensiteettimoduloitu sädehoito, kaarihoito

Preface

I want to express my gratitude to MVision AI for offering this thesis topic, my instructor Gregory Bolard for their continued support and my thesis supervisor Prof. Fabricio Oliveira for their valuable feedback and advice.

Otaniemi, May 27, 2024

Saku Myllymäki

Contents

Symbols and abbreviations

Abbreviations

VMAT	Volumetric modulated arc therapy
IMRT	Intensity modulated radiation therapy
LINAC	Linear accelerator
BEV	Beam's eye view
OAR	Organ at risk
PTV	Planning target volume
MLC	Multileaf collimator
DMPO	Direct machine parameter optimisation
DL	Deep learning

1 Introduction

Cancer is a group of diseases characterised by abnormal growth of cells that have the potential to spread to other parts of the human body. It is a major cause of death throughout the world, especially so in high-income countries. [24]

A group of cells growing in an uncontrolled manner form a tumor, which are the target of treatment for most cancer treatment methods. Depending on the type of cancer, stage of its progression and its location, different treatment methods are used. Some commonly used treatment methods of cancer include surgery, chemotherapy and radiotherapy. [1]

In radiotherapy, high doses of ionising radiation is used to kill cancer cells and shrink tumors. Radiotherapy can be either internal, where a radiation source is placed inside a patient's body or external, where a radiation device shoots ionising through the patient. In this thesis, the focus is on external radiotherapy.

External radiotherapy is commonly delivered by a linear accelerator, a device which accelerates charged particles up to speeds enough to damage the DNA of cancer cells. Most types of cancer are moderately radiosensitive, which means that relatively large amounts of ionising radiation are required to have a curing effect. Some types of cancer might be so insensitive to radiation that the required amounts of radiation would be unsafe for the surrounding organs.

Sparing of surrounding tissue and organs is a major consideration in radiotherapy treatment planning. Modern linear accelerators and treatment planning systems provide various means of planning treatment in a way which spares surrounding organs. This topic will be covered in Sections 2.2.4-2.3.3.

Treatment planning starts with a desired radiation dose for the patient. A doctor prescribes a dose for the target organ and sets radiation limits for the surrounding organs. The aim of treatment planning is to devise a dose delivery plan for the linear accelerator, which delivers a dose with minimum deviation from the desired dose. In practice, surrounding organs receive significant amount of radiation and compromises have to made to achieve the desired dose levels in the tumor. The tradeoff between target coverage and organ-at-risk (OAR) sparing makes dose optimisation a multi-objective optimisation problem.

Since the beginning of treatment planning, increasingly sophisticated and accurate planning methods have been developed. Relevant in modern radiotherapy and this thesis are inverse planning methods, a group of methods in which parameters of the treatment machine are adjusted iteratively with optimisation according to desired dose and physical machine limitations. In inverse planning methods, optimisation objectives based on the desired target dose and OAR dose limits are used to guide an optimiser software to find an optimal dose.

In clinical practice, commercial optimisation software is commonly used for plan creation. A practitioner sets radiation targets for the tumor and limits for surrounding organs according to best clinical knowledge of the type of cancer and the individual requirements and constraints of the patient. Less common in practice is dose mimicking, an approach where instead of target and OAR objectives, the optimiser is guided to get as close to a desired dose grid as possible. This reference dose grid is created with a deep learning model trained on a set of patient cases on which multiple rounds of VMAT (volumetric modulated arc therapy) optimisation were run by a clinical expert to provide high quality training data. Patient data is given to the trained model, which predicts a dose grid of high quality with regards to clinical objectives. It is hypothesised that the dose grid should be close to what can be attained for the patient with optimisation.

In this thesis, one of the goals is to evaluate the potential of dose mimicking, predicted dose derived conventional structure objectives and various hybrid approaches in attaining this dose quality by running experiments on 15 patient cases. These approaches will be described in detail in Section 3.2 and the patient data described in Section 4. Due to the lack of open source VMAT optimisers, IMRT (intensity modulated radiation therapy) was used instead. The effects of using IMRT for dose mimicking on VMAT characteristic dose distributions is discussed in Section 5.2.

Simultaneously, all these approaches enable an automatic workflow for plan creation. The conventional optimisation objectives are automatically derived from the predicted dose for the experiments. In addition, the dose mimicking and hybrid methods utilise the predicted dose for setting up the optimisation process automatically. Indeed, a second goal of this thesis is to devise an automatic procedure for setting up plan optimisation informed by the experimental results.

The conventional objectives derived from the predicted dose were found to perform the best, the reasons for which are discussed in Section 5.2. Informed by these results, it is proposed that conventional objectives derived from the predicted dose can be used to produce doses of almost comparable quality to the predicted dose, even with an IMRT optimiser.

2 Literature review

2.1 Cancer treatment modalities

Abbas and Rehman [1] list four main categories of cancer treatment modalities: surgery, radiotherapy, chemotherapy and hormonal therapy [1]. Surgery and radiotherapy are considered local treatment methods, as they can both be used to treat a tumor located in a specific location of the patient. Chemotherapy and hormonal therapy are systemic treatment methods, which means that they target cancer cells throughout the body.

In the normal functioning of the body, a cell divides around 50 times until it dies. The cell dies as a result of apoptosis, a process in which the body sends a signal for the cell to stop dividing and the cell is replaced by another after its death. Cancer cells exhibit no response to these signals and continue to grow and divide uncontrollably. In addition, cancer cells have the ability to spread to other tissues but not before the cancer tumor has grown sufficiently large. If cancer processes far enough for cancer cells to start invading surrounding tissues, it is very hard to treat and often turns fatal for the patient. Cancer treatment methods may either aim to kill a body of tumor cells or to affect the uncontrollable division behavior of cancer cells throughout the body. [1]

Before 1950, the only cancer treatment considered was surgery. Surgery is an especially promising treatment option for tumors because it assures minimal damage to surrounding tissue, unlike radiotherapy and chemotherapy. Depending on the type of tumor and its location in the body, surgery aims to remove either the whole tumor or the bulk of its mass, leaving the rest of the tumor to be treated by other treatment methods. [1]

Radiotherapy is a collection of treatment methods, in which a dose of ionising radiation is delivered to a tumor. Charged particles interacting with tumor cells can alter their genetic structure to the extent of killing them directly or halting their replication mechanisms [1]. In this thesis, the focus is on external radiotherapy, in which a focused beam of particles is delivered from outside of the body on the target. Radiotherapy will be discussed more thoroughly in Section 2.2.

Chemotherapy affects tumors by removing the ability of tumor cells to divide and enforces their natural death. However, chemotherapeutic drugs also affect normal cells, leading to various serious side effects. With high enough doses, these drugs can affect the immune system, which can eventually lead to complications or even death of the patient.

Abbas and Rehman [1] also report numerous other treatment methods, including hormonal therapy, various radiation modalities and agents capable of disrupting the cell cycle or cell division, falling to the same category with chemotherapy. In their report on cancer treatment modalities, Zadeh et al. [18] also note that different treatment modalities, such as surgery and radiotherapy, can be used jointly to achieve better results.

As previously stated, this thesis will focus solely on radiotherapy. However, regardless of whether a patient has previously undergone a surgery or received chemotherapy, the underlying process for radiotherapy planning is the same. Previous treatment history is accounted for by practitioners by the radiation targets and limits they set for organs and the tumor and by designing the planning target volumes appropriately.

2.2 Radiation therapy

2.2.1 Beam production

Ionising radiation delivers biological damage to cells by breaking molecular bonds, which damages DNA. Photons from the radiation source interact with matter, producing high energy electrons. These electrons travel through tumor tissue, interacting with both water molecules around cells and the cells directly. Electrons interacting with water molecules produce highly reactive water ions and hydroxyl radicals. Both water ions and hydroxyl radicals are reactive ions which have the potential to affect chemical bonds in the radiation target. This can induce various biological effects on cancer cells, killing them or affecting their ability to reproduce. It is worth noting that ionising radiation has the potential to induce cancer and this effect can be delayed by years after exposure to radiation. [33]

2.2.2 Linear accelerators

The advent of radiotherapy dates back to the year 1895, when X-rays were discovered by Wilhelm Röntgen. During the 20th century, new radioactive isotopes and radiation techniques were discovered and scientists would gain understanding of the effects of radiation dose on cell survival, aiding the development of radiotherapy treatments. Eventually, the development of dose delivery machines lead to electron linear accelerators, which would be able to deliver megavoltage X-rays. These megavoltage X-rays would have high enough particle energies to penetrate the skin and give high doses to deep tumors. [14]

The initial electron beam is generated by accelerating electrons through an electric potential difference. Medical linear accelerators are cyclic accelerators, which means that electrons go through the same linear path with the potential difference multiple times, gaining energy each time. Although the initial beam consists of electrons, the X-ray is produced by the electron beam hitting a medium, usually a target made of tungsten. Electrons from the initial beam displacing electrons of the target material produce characteristic X-rays, emitted in the form of photons. Characteristic X-rays are the result of Coulomb interactions, in which electrons of the atoms in the target material are displaced from their orbit. An electron from a higher shell fills the vacant orbit, releasing a discrete amount of energy equivalent to the energy difference between the shells. Tungsten is a particularly appealing material due to its high atomic number, which makes high energy characteristic X-rays possible. Another type of

X-ray resulting from electrons hitting the target material is a bremsstrahlung ray, which has a continuous spectrum of energy. This kind of X-ray is the result of interaction between electrons and atom nuclei. The electron decelerates and its loss of kinetic energy is released in the form of bremsstrahlung photons. Some linear accelerators can be used to produce electron beams by not using an X-ray target [33]. However, electron beams are of less relevance in this thesis and will not be discussed.

According to Podgorsak [33], linear accelerators consist of five major parts: gantry, gantry support, treatment table, modulator cabinet and control console. Gantry is the part along which the radiation source rotates, supported by the gantry support. Treatment table is where the patient lies. The modulator cabinet is a component that produces electrical power and high-voltage pulses required for electron acceleration.

In the next section, the focus will be on beam modifiers, the moving parts in the head of the treatment device which are used to shape beams for finer targeting of the tumor and surrounding tissue.

2.2.3 Beam modifiers

The head of the treatment device consists of parts used for production of photon beams and shaping, localising and monitoring both electron and photon beams. Leaving aside the details of how clinical beams are produced, mostly relevant for beam shaping are the several collimators, which act by absorbing incident radiation. The primary collimator narrows the beam down to a circular beam. Two horizontal and vertical jaws further narrow it to a rectangular beam. Finally, the multileaf collimator (Figure 1), a collection of moving tungsten plates, can be used to shape the resulting beam to more complicated and clinically useful shapes. [33]

Modern linear accelerators have from 20 to 80 pairs of narrow tungsten leaves, with a typical width of around 10 millimeters. Each leaf is individually controlled by a computer, allowing irregular beam shapes accurately conforming to target structure shape. [9]

2.2.4 Treatment planning

Organs exhibit different responses to ionising radiation. Too much radiation to any organ has the risk of causing side effects more serious than the cancer to be treated. Different organs vary in their ability to withstand radiation. The ideal is to give zero radiation to all OARs, while giving the exact amount of radiation for the target required to treat the tumour. In practice, however, this objective is impossible and compromises have to be made. It is the job of the practitioner to determine safe limits of radiation for each organ depending on the patient, the type of cancer and pre-existing conditions of the patient. Based on these limits, treatment plans can be created.

The radiation beam emitted from the treatment machine is initially a rectangular field of uniform intensity. Without any shaping of the field, the beam will not be

Figure 1: A multileaf collimator consists of radiation absorbing tungsten leaves, which can be moved individually allowing complex beam shapes. Picture from Varian Medical Systems, Palo Alto, California. [Source: Bortfeld [4]]

entirely concentrated on the tumor, but will give unnecessary radiation to tissue around the tumor. This issue creates the need for conformal therapy, in which beam shape is modulated to conform to the tumor shape. According to Fraass [12], Takahashi [43] was the first to describe the use of "geared sectional collimators", mechanical devices used to conform to treatment target shape, utilising 3D models of the tumor to plan the conformal treatment. These devices were the early version of the modern multileaf collimators, described in the previous section.

When treating a patient with radiation, the beam will first pass through tissue and organs in front of the target, deliver radiation to the target and continue, dispersing energy not only on the tumor to be treated but through a whole section of the patient's body. To avoid irradiating a particular organ past safe limits, multiple beams from different directions can be used. The beams are all centered on the tumor, which is aligned with the axis of rotation of the gantry. Each beam can be less intense or of shorter duration, which reduces radiation on organs around the target while the target receives the full dose. For these reasons, treatment planning procedures utilise gantry rotation or several beam angles and multileaf collimation to create treatment plans.

Rotational dose delivery is a relatively old idea, first suggested by Kohl [21]. Brahme et al. [6] were the first to pose treatment planning as an inverse problem. Their

paper asks the question - which radiation intensity distribution from the incoming beam produces a uniform dose distribution in a cylindrical target volume? Bortfeld [4] describes this paper as the one which 'invented' IMRT, a topic of a subsequent section. In a modern setting, characterised by abundant computational resources and computerised control of various linac features, inverse planning encompasses finding optimal gantry positions and speeds, leaf positions and beam intensities iteratively by optimisation methods. The term "inverse planning" hints to its separation from the traditional forward planning approach, where plan parameters are manually set according to the best subjective knowledge of the practitioner giving the treatment.

Modern linear accelerators have the capacity to deliver treatment plans with varying gantry speed and dose rate, which allow more fine tuned treatment plans. The degree of complexity and interplay between these features allows for more conformable plans but also makes treatment planning more complicated [7]. To devise treatment plans by inverse planning, two elements are crucial: dose calculation and optimisation methods. These will be the topics of subsequent sections.

2.2.5 Treatment quality evaluation

Modern treatment planning techniques can provide highly conformal treatment plans, but how exactly is the plan quality assessed? The evaluated quality of a dose is highly dependent on the patient, the type of cancer treated and the organs surrounding the tumor. It is up to the radiation oncologist to inspect the distribution of radiation received by the PTV and OARs for quality control.

A common tool used by practitioners for plan evaluation is the dose volume histogram (DVH). Dose volume histograms can also be used to compare doses resulting from two different treatment plans, as illustrated in Figure 2.

Doses can also be visualised on every 2D slice of the patient by coloring each pixel according to dose intensity. DVH curves reduce the three dimensional spatial information of the dose to two dimensions, losing information in the process. Hence a slice-by-slice inspection of the dose is recommended in [17].

Determining safe limits for radiation on OARs is an extremely complex problem. Dr. Emami [11], in a report on tolerance of normal tissue to radiation, summarises complications arising from irradiation of different organs and corresponding recommendations for radiation limits. Even these limits, as stated in the report, can vary from patient to patient as a higher risk of complications could be accepted to improve the likelihood of a certain treatment outcome. In the end, radiation limits need to be decided by the practitioner not only considering clinical outcomes, but also preferences of the patient being treated.

The previous statement underlines the multi-objective nature of dose optimisation. This tradeoff between tumor control probability (TCP) and normal tissue complication

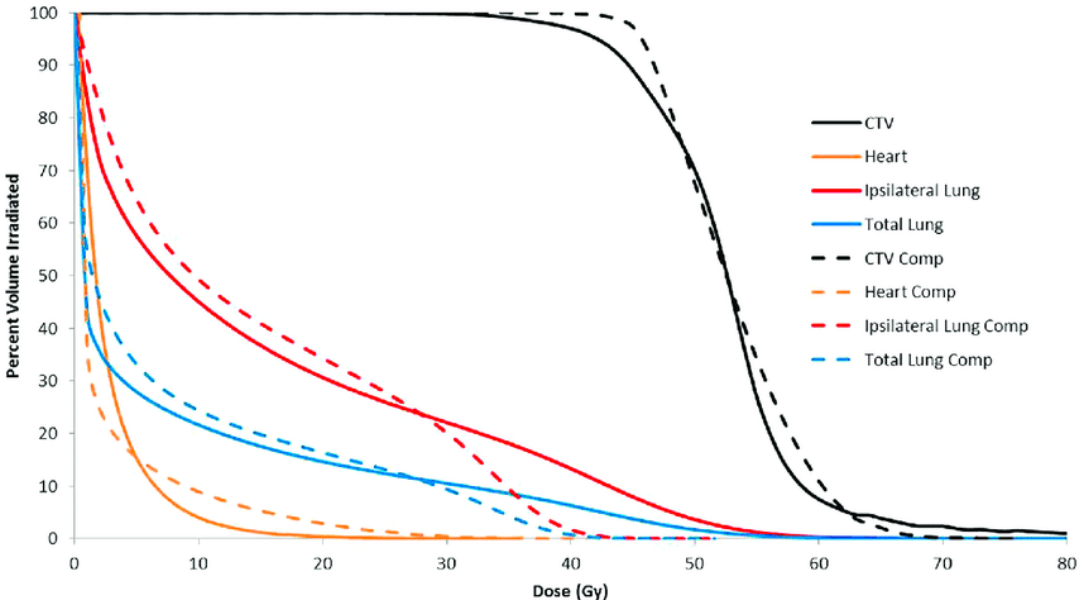

Figure 2: An example DVH with two plans compared [Source: Craft et al. [10]]

probability (NTCP) is often illustrated with a graph of the therapeutic radio, shown in Figure 3. The TCP and NTCP are modelled to take into account biological effects of radiation on cells, estimating probabilities of killing the tumor and producing complications in normal tissue, respectively [30].

Metrics derived from the DVHs are also useful and can be simpler to interpret than DVH curves themselves. Such metrics are minimum, maximum and mean dose on the PTV and OARs. The ICRU Report 83 by Grégoire and Mackie [15] recommends reporting the 98th and 2nd quantile of the dose for maximum and minimum doses for better statistical significance. In addition, homogeneity indices report the uniformity of dose in the PTV, conformity indices measure the ratio of high doses on the PTV to high doses on normal tissue while gradient indices measure the steepness of dose falloff around the PTV. A homogeneity index and conformity index in addition to the mean and 99th quantile dose are also reported for the experimental results of this thesis and explained with more detail in Section 5.1.

2.3 Dose optimisation

2.3.1 Structure delineation

For optimisation and dose calculation purposes, the patient geometry information is stored as a three-dimensional grid of voxels, which are small rectangular cuboid volume elements. This information is generally obtained by magnetic resonance imaging (MRI) or computational tomography (CT) and further sampled or interpolated for desired grid resolution. In order to create optimisation objectives for the tumor or OARs, borders are generally drawn by practitioners or automatic tools around these volumes of interest (VOI) on the MRI or CT images. Based on these delineated areas

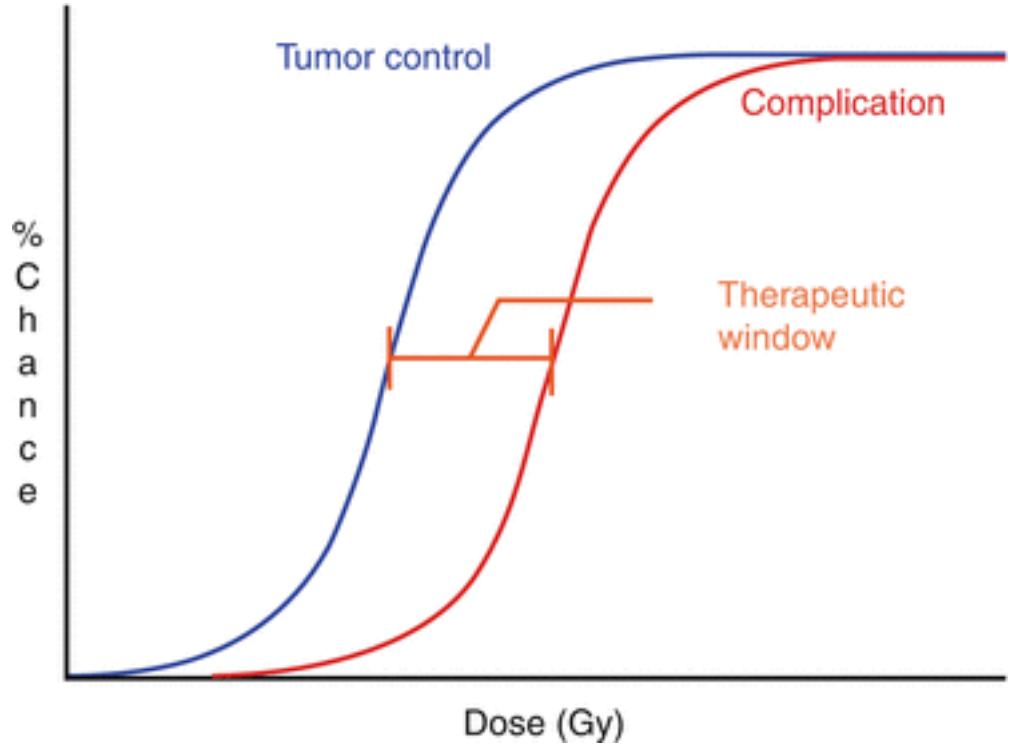

Figure 3: Relationship between tumor control probability and normal tissue complication probability [Source: Chang et al. [8]]

in each image, 3D volumes corresponding to each volume can be created. All VOIs then take up a set of voxels in the grid.

There are essentially two ways to define dose objectives: per-volume or per-voxel. Per-voxel dose is simply desired dose for each voxel, and can be described as a vector consisting of the desired dose each voxel in the planning volume. In practice, however, defining voxel-based doses might be difficult and are usually generated automatically as in the dose prediction model used in this thesis. Volume objectives are generally defined on the whole organ volume, and objectives such as max or mean dose or EUD objectives are defined on a per volume basis. The objectives used for optimisation will be more thoroughly discussed in Section 3.2.

2.3.2 Intensity modulated radiation therapy (IMRT)

IMRT is a dose delivery technique involving several fixed gantry positions, the number and angles of which can be decided by the practitioner. In his IMRT review paper, Bortfeld [4] decribes IMRT as treatment planning methods where intensities of incoming beams are modulated to conform to the target and surrounding organ objectives and the multiple beam directions complement each other, accounting for cold and hot spots of other beams. A schematic drawing of IMRT is shown in Figure 4.

The process for optimising an IMRT treatment plan is generally realised in two distinct

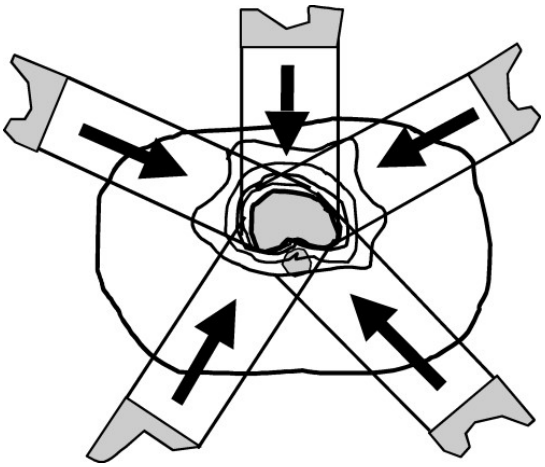

Figure 4: IMRT with multiple beam angles and beam intensity distributions visualised. [Source: Metcalfe et al. [26]]

steps - fluence optimisation and leaf sequencing. Fluence optimisation is the process of optimising the beam intensity distributions from each incoming beam and leaf sequencing is the subsequent step of finding leaf positions and movement patterns conforming to the optimised fluence maps as closely as possible. Both topics will be handled in more technical detail for the specific approaches used in the experiments of this thesis.

Fluence optimisation starts with discretising each beam to a two-dimensional grid of beamlets - small rectangular sections of the whole beam. Each beamlet results in an individual dose contribution in the body, and the intensity (amount of radiation) passing through each beamlet can be individually optimised to find an optimal intensity distribution for each beam. The calculation of the contribution of each beamlet in a body made of heterogeneous tissue is a complex topic and will be addressed in Section 2.3.4.

The optimised intensity distributions represent ideal beams and are generally not attainable with a multileaf collimator (MLC), as the moving plates are not able to modify the incoming beam to arbitrary intensity distributions. Various strategies for leaf sequencing exist. Saw et al. [34], identify the two main strategies for leaf sequencing in IMRT - the static "step-and-shoot" technique and dynamic leaf sequencing. Figure 5 illustrates an optimal fluence map and a single MLC segment.

In static leaf sequencing, the optimal fluence map is stratified to a number of levels of intensity, and the leaf sequencing algorithm tries to find a minimal number of leaf positions, also called segments, whose sum corresponds to the discrete levels. Each segment is delivered separately and radiation is turned off during leaf movement.

In dynamic leaf sequencing, the leaves are allowed to move while radiation is being delivered, allowing wedge-shaped intensity distributions. As described by Saw et al. [34], "the intensity pattern is decomposed into a series of segments such that the

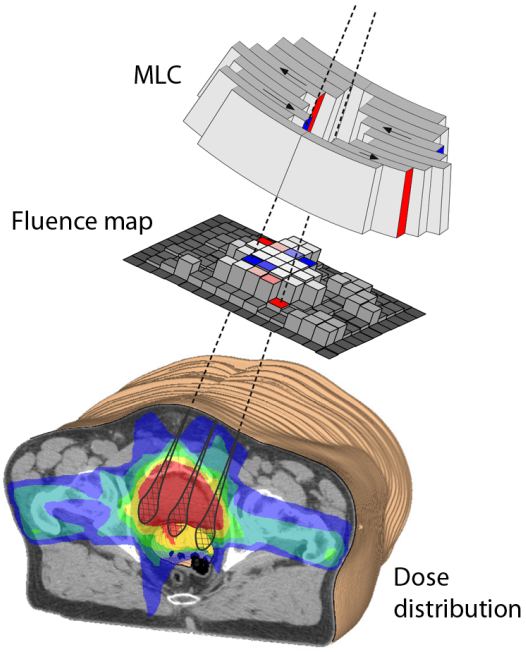

Figure 5: Drawing of a fluence map and a single segment of MLC leaf positions. The desired fluence map can generally not be delivered by a single segment. [Source: Siggel [40]]

leaf positions in one segment are related to those of the next segment by leaf velocity constraints and unidirectional motion". This kind of delivery technique provides shorter delivery times than with static sequencing, albeit prone to leaf-positional errors.

For static leaf sequencing after the sequencing step, the leaf positions can be further optimised with direct machine parameter optimisation (DMPO). This includes optimising each leaf position for each segment directly to account for decrease in dose quality after the sequencing step. DMPO was originally designed to replace the fluence optimisation and leaf sequencing step [36], using a simulated annealing approach for finding suitable segments, given beam angles, energies and segments per beam as a starting point. In the experiments conducted in this thesis in Section 5, however, DMPO was used after leaf sequencing as a separate optimisation step.

2.3.3 Volumetric modulated arc therapy (VMAT)

Treatment times required for delivering IMRT plans, depending on the number of beam angles and segments used, can be too long for sufficient throughput in clinics. VMAT was originally invented by Karl Otto [32] to overcome this issue.

The new type of treatment featured dose delivery while the gantry is rotating a full 360 degree round. In theory, the added freedom of beam angles should result in higher quality doses. However, the deliverable segments between consequent angles

need to be close enough to account for maximum leaf travel speeds. Furthermore, the design of the linac and its components pose additional constraints, including maximum and minimum dose rate and maximum gantry rotation speed.

The idea and practical implementation of modulating the field shape while the gantry is rotating was first conceived by Yu [45], who designed intensity modulated arc therapy (IMAT), a precursor to VMAT using multiple superimposed arcs. According to Otto [32], IMAT has several issues producing an accurate and deliverable plan. Optimisation of leaves while the gantry is moving is generally done with coarse sampling at angle increments of 5-10 degrees and leaves can travel significantly between subsequent angles. Too coarse angle sampling and significant leaf movement between angles can cause large differences between optimised and delivered dose due to errors in dose calculations [32, 37]. These issues were the original motivation of developing VMAT.

Similarly, the approach proposed by Otto [32] starts with fluence optimisation and leaf sequencing for each beam direction. Initial sampling is coarse and can be done for intervals of 10 degrees. After initial optimisation, additional beam shapes are added between the optimised ones by linear interpolation and the leaf positions are then optimised directly, taking into account leaf travel and dose rate constraints. This is similar to DMPO described in the previous section, but with machine imposed constraints. In order to achieve adequate dosimetric accuracy, the final sampling needs to be at intervals of at most 1 degree. Such a number of beam directions to optimise naturally makes the problem computationally challenging and in order to make the total optimisation time feasible, the number of optimisation iterations for each direction is reduced as the number of beam directions increases.

The main advantage of VMAT over IMRT is the reduced treatment time: the treatment plan is delivered with a single arc in constant motion whereas IMRT generally uses a large number of beam directions with multiple MLC segments for each direction. In addition, delivering radiation while the gantry rotates has the potential to provide more conformable doses and avoid excessive dose on OARs, as every beam direction is utilised. The resulting dose distributions are significantly different, as illustrated in Figure 6.

2.3.4 Dose calculation

Given a gantry angle, patient geometry and center of gantry rotation, a dose calculation algorithm computes the resulting dose inside the patient. The dose is calculated for every beamlet (alternatively, pencil beam) separately. That is, for every portion of the beam grid a dose calculation algorithm approximates the dose in every voxel inside the patient. Technically, the dose calculation procedure calculates a matrix D, whose element in the ith row and jth column is equal to the radiation absorbed by jth voxel as a result of delivering a unit intensity of radiation with beamlet i. This is the dose format required for dose optimisation purposes but the calculation can be done with

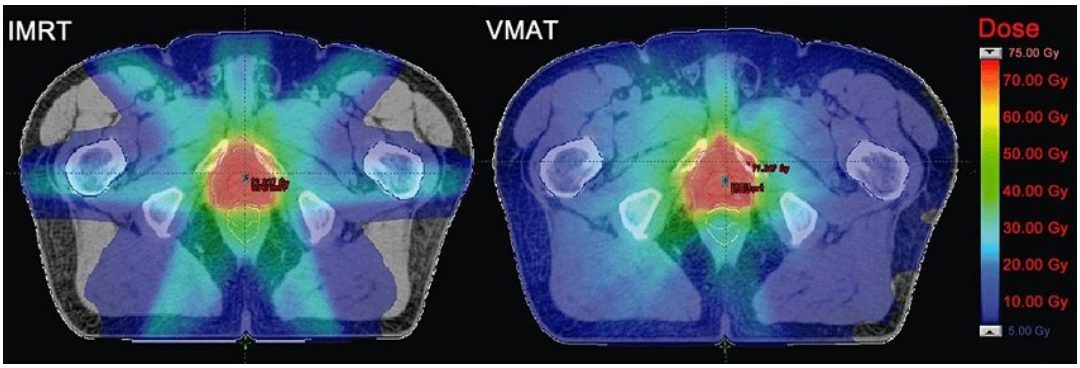

Figure 6: Comparison of dose distributions for IMRT and VMAT plans, demonstrating the effect of constant radiation during gantry rotation. [Source: Nguyen et al. [27]]

various different methods and is generally computationally intensive.

Essentially, a dose calculation algorithm takes as input the intensity distribution of the incident beam and calculates the distribution of energy deposited in the body taking into account patient tissue heterogeneities and interaction of photons with the tissue. Photons exiting the treatment head interact with the treatment head components and patient tissue, causing various forms of energy deposition in the patient.

Ahnesjö and Aspradakis [2] describe four types of dose resulting from a photon beam. These types are described in figure 7 as primary photon dose, treatment head scatter, contaminant particles and phantom scatter.

Primary photon dose is the energy dispersed in the body as a result of photon absorptions into electrons in the target material. The main source of direct photon absorption at low photon energies is the photoelectric effect [33]. At higher energies pair production, an event where a photon interacts with an atom nucleus to produce a proton-electron pair, is more prominent. Pair production also leads to the annihilation of the proton with a free electron, producing two opposite direction photons. In Compton scattering, a free electron is scattered by an incoming photon while the photon changes direction. Compton scattering dominates at intermediate photon energies. [33]

Phantom scatter refers to photons scattered inside the patient. As mentioned previously, Compton scattering and pair production are sources of secondary photons with direction differing from the original beam direction. In Rayleigh (coherent) scatter, a low-energy photon hits an atom, not displacing any particles or losing energy but changing direction. [33]

Treatment head scatter is the photon scatter resulting from photon interactions in parts of the treatment head, such as the collimator or the flattening filter. The scattered photons enter the treatment body and have similar interactions at the primary beam, but the irregular directions and changed intensities of the scattered photons add a com-

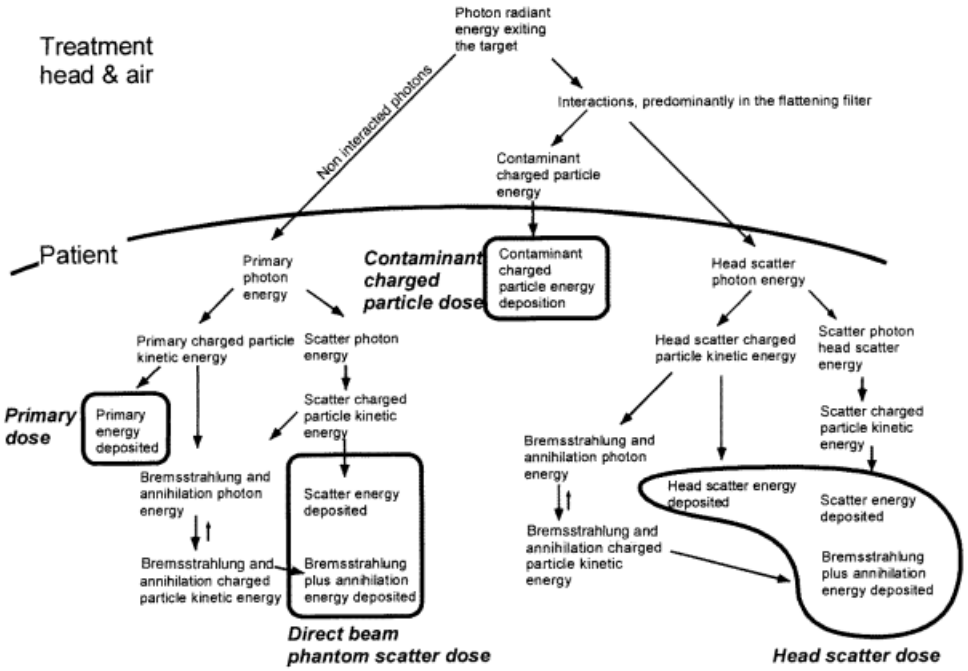

Figure 7: Types of dose resulting from photon irradiation and scatter effects. [Source: [2]]

ponent to the dose that needs to be accounted for in treatment planning. Contaminant particles are charged particles from the treatment head or the air between the treatment head and the treated body.

Radiation energy deposited is generally measured in Grays (Gy), the amount of energy in Joules absorbed per mass in kilograms. Photons transfer their energy to electrons and proton-electron pairs as kinetic energy and charged particles transfer their energy in further interactions. There are different ways of quantifying the transfer of the indirectly ionising photon radiation depending on the accuracy wanted for dose measurements. According to the International Commission on Radiation Units and Measurements (ICRU) report 85 [31], the absorbed dose is the sum of all energy deposition interactions, by charged or uncharged particles, in a mass dm of material. A common approximation is the KERMA (kinetic energy released per mass), which is limited to energy transferred by uncharged particles.

Accuracy and speed of dose calculation are major considerations when selecting a dose calculation algorithm for treatment planning. A good dose calculation algorithm is such that it is able to model the aforementioned particle interactions and the resulting energy distribution with sufficient accuracy while being fast enough to be usable in a clinic.

A common approach for dose calculation in IMRT divides beams into beamlets,

as explained in Section 2.3.2. For optimisation purposes, the contribution of each beamlet to the dose is computed separately. An accuracy concern arising from this approach is that the contribution of each beamlet can not be decoupled from MLC leaf positions, as each MLC leaf lets some radiation through and causes scattered radiation. Radiation through the leaves can be a significant source of radiation [20].

Inaccuracy in dose calculation used for optimisation can cause significant inaccuracy in the final dose after convergence [35]. To counter this issue, many approaches involve using a lower accuracy dose calculation algorithm for most iterations and either correction by a more accurate algorithm for subsequent iterations or final convergence exclusively with the higher accuracy algorithm [35, 38].

In Monte Carlo algorithms, a large number of particle tracks are simulated from the treatment head to the body, modeling first principles of particle interactions. With this approach, Monte Carlo algorithms should theoretically provide best dose calculation accuracy when simulated with high enough number of particles and several studies have used a Monte Carlo dose as a benchmark for more approximative algorithms [3, 22, 13].

The high number of simulated particles needed for sufficient accuracy is computationally challenging and can be too time-consuming for practical purposes. To reduce computational requirements, several algorithms have been developed which use kernels to approximately describe the energy dispersion by secondary photons and electrons from the primary interaction site. These methods are called convolution methods. If the algorithm further takes into account heterogeneities in the media, it is called a convolution-superposition algorithm [23].

2.3.5 Voxel based optimisation

Dose optimisation objectives are traditionally defined on OARs and the PTV and the objectives are balanced by a practitioner to provide an acceptable dose distribution. The approach in this thesis was to use a deep learning (DL) predicted dose distribution on the whole body and attempt to mimic it with various optimisation methods.

The most important benefit from using dose mimicking is the elimination of the need of a practitioner in the dose optimisation step, increasing patient throughput and potentially producing higher quality doses [25, 19]. The idea of dose mimicking is not new: McIntosh et al. [25] trained several machine learning models for predicting dose distributions and applied dose mimicking with fixed beam settings for both IMRT and VMAT. They had promising results with the mimicked doses nearly consistently outperforming clinical doses. However, they also recognised the necessity of a dose prediction technique capable of producing a dose distribution which is realistic for the optimiser and treatment machine to achieve.

A recent work by Kadoya et al. [19] explored the use of dose structures based on a DL predicted dose, and concluded that treatment plans generated using these

structures were clinically acceptable after being reviewed by practitioners, and in some regards even of higher quality than benchmark clinical plans.

The aim of this thesis is to find the best optimisation strategy to be used together with MVision's DL predicted dose distribution and to test the usability of the predicted dose distribution for optimisation purposes. The experimental part explores using pure voxel mimicking and generated optimisation objectives based on the predicted dose.

3 Methods

3.1 Optimisation problem formulation

3.1.1 Fluence optimisation

Denote by D the dose influence matrix, with D_{ij} being the dose delivered to voxel i through beamlet j by unit amount of radiation through the beamlet. Let τ be the vector of beamlet weights. Then, the dose to voxel i is given by $D\tau$.

Let f denote the objective function, which is a weighted sum of several objective functions optimising the dose to the PTV and minimising the dose to the OARs and normal tissue around the PTV. Various objectives are explored, and the exact functions used are discussed in Section 3.2. In addition, dose optimisation might involve constraints on the dose, but they are not explored in the experiments conducted in this thesis.

In traditional IMRT, the first optimisation problem is to solve

$$\begin{aligned} &\min_{\tau} f(D\tau) \\ &\tau \geq 0, \end{aligned}$$

where the non-negativity requirement for τ prevents negative radiation amounts.

In this approach, the main problem is that the optimised fluence maps τ might not be deliverable with the machine in use, because it does not take into account leaf movement. To create deliverable plans, leaf sequencing based on the optimised fluences τ must be applied.

3.1.2 Leaf sequencing

The leaf sequencing algorithm used in these experiments is a static sequencing algorithm by Siochi and Alfredo [41]. This approach discretises fluence levels of beamlets to desired accuracy and finds an optimal combination of beam shapes and radiation durations conforming to the discretised fluences. Following an example from [41], assume for simplicity an (unrealistic) beam with 3 pairs of leaves and a 3x5 discretisation to beamlets. Assume further that the fluences are discretised to 9 intensity levels and the intensities are rounded to yield the following total beam durations:

$$\begin{bmatrix} 5 & 7 & 9 & 8 & 6 \\ 5 & 7 & 7 & 7 & 6 \\ 1 & 4 & 4 & 4 & 1 \end{bmatrix}$$

Then a set of leaf position used to deliver such an intensity distribution could be, for example

$$\begin{bmatrix} 5 & 7 & 9 & 8 & 6 \\ 5 & 7 & 7 & 7 & 6 \\ 1 & 4 & 4 & 4 & 1 \end{bmatrix} = 3 \begin{bmatrix} 1 & 1 & 1 & 1 & 1 \\ 1 & 1 & 1 & 1 & 1 \\ 0 & 1 & 1 & 1 & 0 \end{bmatrix} + \begin{bmatrix} 1 & 1 & 1 & 1 & 1 \\ 1 & 1 & 1 & 1 & 1 \\ 1 & 1 & 1 & 1 & 1 \end{bmatrix} + \begin{bmatrix} 1 & 1 & 1 & 0 & 0 \\ 1 & 1 & 1 & 1 & 0 \\ 0 & 0 & 0 & 0 & 0 \end{bmatrix}$$
$$+2 \begin{bmatrix} 0 & 1 & 1 & 1 & 0 \\ 0 & 1 & 1 & 1 & 1 \\ 0 & 0 & 0 & 0 & 0 \end{bmatrix} + 2 \begin{bmatrix} 0 & 0 & 1 & 1 & 1 \\ 0 & 0 & 0 & 0 & 0 \\ 0 & 0 & 0 & 0 & 0 \end{bmatrix}$$

The binary matrices represent deliverable beams: 1 is for beamlets not blocked by MLC leaves and 0 is for blocked beamlets. The algorithm takes into account certain limitations on leaf movement, such as discontiguity and leaf collisions in addition to tongue and groove effects.

3.1.3 Direct machine parameter optimisation

In direct machine parameter optimisation (DMPO) [16], the approach is to solve the following optimisation problem:

$$\begin{aligned} &\min_{x,w} f(d(x,w)) \\ &\text{s.t. } Ax \leq b \\ &\quad w \geq 0 \end{aligned} \tag{1}$$

In this approach, each beam is divided into control points, and each control point is described by a vector of leaf positions x and a segment weight w. The function $d(x,w)$ calculates the dose resulting from the given leaf positions and segment weight for a beam. In the optimisation problem (1), the leaf positions for all control points of all beams are collected to the vector x and segment weights of all control points are collected to the vector w. Then $d(x,w)$ is the dose received by the patient and $f(d(x,w))$ is the objective function. The constraint $Ax \leq b$ ensures that the leaf positions x are achievable by the machine, and $w \geq 0$ prevents negative fluences.

Although in this thesis DMPO is restricted to shaping individual segments, it readily extends to VMAT: The control points are simply set up for different angles and the constraint $Ax \leq b$ needs to take into account gantry speed and maximum leaf movement per gantry angle rotation for subsequent leaf positions.

3.2 Optimisation methods

3.2.1 Conventional objective generation

Conventional objectives or volume objectives, as mentioned previously, are optimisation objectives defined on volumes corresponding to organs or the treatment target. There are different types of constraints or objectives one can define for the dose of

each volume. Some common ones include maximum dose, minimum dose, mean dose and dose-at-volume.

Maximum, minimum and mean dose are self-evident. Similarly to dose quality evaluation in Section 2.2.5, the 99th quantile was used for the maximum dose also for the optimisation objectives. While maximum and mean dose are used to limit radiation to all volumes, minimum dose is used for the PTV to ensure a certain amount of radiation. However, minimum objectives were not used for the experiments. The dose-at-volume is the minimum amount of radiation d absorbed by a specified percentage of volume, denoted by $DV_p(D) = d$, where D is the dose at every voxel in the given volume and p is the percentage. This means that $p\%$ of the volume receives at least d amount of radiation. The dose-at-volume objective can be used to allow the given dose d to at most $p\%$ of the volume, but is penalised or strictly restricted if too many voxels of the volume receive more than d.

Which kind of dose objectives should be used depends on the type of organ in consideration. Depending on the dose distribution and the organ, the biological effects caused by the radiation may vary greatly. Niemierko and Goitein, in their report, characterise organs as a collection of functional subunits [29]. Some organs, called serial organs, fail when a single functional subunit is destroyed. An example of such an organ is the spinal cord. Parallel organs are more graded in their response to radiation absorbed. These are important considerations for practitioners when choosing optimisation objectives and evaluating plans.

A type of dose objective well suited for handling different types of organs is the equivalent uniform dose (EUD), which tries to approximate the amount of dose that would have the same biological effect to the organ if distributed uniformly to the entire volume. Niemierko [28] defines the EUD as

$$EUD_{D,a} = \left(\frac{1}{N}\sum_{i=1}^{N} d_i^a\right)^{\frac{1}{a}},$$

where N is the number of voxels in a given volume with dose D, d_i is the dose received by voxel i and a is called the volume parameter, which is used to model the biological effects of different dose distributions and organs.

A large value for a corresponds to an organ which has low tolerance for high dose values anywhere in the organ (serial organ). A value $a = 1$ corresponds to the mean dose and a value less than one has the effect of giving larger weights for low doses. This could be useful for target volumes when trying to avoid cold spots in the delivered dose [42]. Determining the value of a for different organs can be difficult in practice and requires extensive knowledge about the biological effects different radiation distributions have on different organs.

For the automatic objective generation, two EUD objectives with $a = 1$ and $a = 3$ and

a dose-at-volume objective with $p = 1$ were created based on the corresponding values from the predicted dose distribution for each OAR. During the optimisation, a dose exceeding the reference values was penalised with squared deviation. Formally: let D_{pred} be the DL predicted dose and $D_{pred,OAR}$ the predicted dose restricted to a given OAR. Then the EUD and dose-at-volume values are $EUD_{D_{pred,OAR},1}$, $EUD_{D_{pred,OAR},3}$ and $DV_1(D_{pred,OAR})$, respectively. For brevity, denote them by a_1, a_3 and b.

Now consider a dose distribution D to the OAR during optimisation. Denote by $c = DV_1(D)$ the dose-at-volume value of D in OAR, that is, the 99th quantile of D. Ideally, $c \leq b$ and the objective function takes a positive value when $c > b$. Then the following objective function was defined for the OAR:

$$g_{OAR}(D) = g_{OAR,EUD_1}(D) + g_{OAR,EUD_3}(D) + \frac{1}{N}\sum_{i=1}^{N} g_{OAR,D_1}(d_i)^2,$$

where

$$g_{OAR,EUD_1}(D) = \begin{cases} 0, & EUD_{D,1} \leq a_1 \\ (EUD_{D,1} - a_1)^2, & EUD_{D,1} > a_1 \end{cases}$$

$$g_{OAR,EUD_3}(D) = \begin{cases} 0, & EUD_{D,3} \leq a_3 \\ (EUD_{D,3} - a_3)^2, & EUD_{D,3} > a_3 \end{cases}$$

$$g_{OAR,D_1}(d_i) = \begin{cases} 0, & d_i \leq b \text{ or } d_i \geq c \\ (d_i - b)^2, & b < d_i < c, \end{cases}$$

d_i is the dose to a single voxel and N the number of voxels in OAR. The intuitive meaning of the last objective is that any dose exceeding the reference dose-at-volume value b of the predicted dose but not above the 99th quantile dose in the OAR will be penalised.

For the PTV, the average squared deviation from the prescribed dose level is used and weighted by 20 to give sufficient importance for target dose homogeneity, that is, higher conformity to the prescribed dose value in the target. It is a topic of later discussion whether this weight was sufficient.

In addition to PTV and OAR objectives, normal tissue objectives (NTO) were added around the PTV to induce a sharper dose gradient around the PTV. This mitigates leakage of high doses to surrounding areas. The NTOs, defined as rings of equal margin around and with increasing distance from the PTV, approximate an exponential falloff function:

$$f(x) = \begin{cases} f_0 e^{-k(x - x_{start})} + f_\infty(1 - e^{-k(x - x_{start})}), & x \geq x_{start} \\ f_0, & x < x_{start}, \end{cases}$$

where f_0 is the start dose near the surface of the PTV, f_∞ is the end dose far from the surface, x_{start} is the width of the margin around the PTV and x is the distance from

the surface of the PTV. Controlling the sharpness of the dose gradient, k is the falloff parameter.

For the experiments, f_0 was defined as 95% and f_∞ as 25% of the prescribed dose. The value for k was defined such that $f(x)$ is 50% of the prescribed dose at $x = 20$ (mm) and x_{start} was set to 2mm. Rings of 3mm width were created for the PTV and dose exceeding $f(x)$ was penalised with squared deviation, where x is the distance of the inner surface of the ring from the surface of the PTV. Rings were created up to a cumulative margin of 30mm.

3.2.2 Full voxel mimicking

In the full voxel mimicking approach, a voxel-based squared deviation objective was used for the PTV and voxel-based squared overdosing for the rest of the body. The objective function definition is similar to the conventional objectives in the previous section for the OARs.

3.2.3 Partial voxel mimicking

Similarly to full voxel mimicking, the partial voxel mimicking approach uses squared deviation and overdosing for the PTV and OARs but ignores the voxels lying outside of the PTV and OARs. Partial voxel mimicking is also named as "labels voxel mimicking" in the graphs in Section 5.2.

3.2.4 Hybrid approaches

Added as a countermeasure for poor target homogeneity in the voxel mimicking approaches, the two hybrid approaches replace the squared deviation from the predicted dose to squared deviation from prescribed dose level in the PTV. Voxel based dose mimicking is still applied for the rest of the body. In addition, the second hybrid approach uses the normal tissue objectives also used in the conventional approach to induce a sharper dose gradient around the PTV.

4 Case-study setup

4.1 Patient data sets

The experiments were performed on 15 patient cases, including 4 prostate, 3 head and neck, 2 pelvis, 5 bone and 1 lung cases. Each dataset contains CT images of the patient, which is required for dose calculation inside the patient as a detailed description of patient anatomy is necessary for dose calculation. In addition, each dataset contains a structure file, a plan file and a dose file. The structure file contains contour information of the PTV and each of the organs, which essentially enables the optimiser to know which voxels of the patient are part of which organs. This is essential information for objective function definitions. The plan file contains relevant metadata for the optimisation procedure and the dose file contains the predicted dose matrix.

4.2 Dose predictions

For each dataset, a dose is predicted using MVision's dose prediction model. The model is a deep learning model, trained with patient data created by a clinical expert. The data was curated by running optimisation to obtain a high quality dose by fine tuning VMAT optimisation objectives in an iterative trial-and-error approach. This process was repeated for numerous cases to create a training dataset for the model, which learns to predict a dose matrix given patient data. This dose matrix is used as a benchmark for all the optimisation experiments and as the target dose distribution for the voxel mimicking approaches.

4.3 Tools

MatRad, a radiotherapy planning toolkit developed by Wieser et al. [44], was used for the experiments. For dose calculation, a pencil beam kernel algorithm described by Bortfeld et al. [5] is implemented in MatRad following the details of [39]. The algorithm relies on a kernel decomposition approximation and tissue heterogeneity approximation with radiological depth tracing. As a pencil beam algorithm, it is prone to significant errors when tissue heterogeneity is present and should not be used as the sole dose computation algorithm for dose optimisation in a clinical setting. As the goal of this thesis is not to create clinically acceptable treatment plans, this mainly limits the accuracy of the results of the experiments [35].

The dose calculation relies on base data obtained with a clinically approved photon dose calculation engine [44]. The base data includes parameters of the decomposed lateral scattering kernels and depth dose components for a generic 6MV linear accelerator. As such, the dose calculation does not necessarily reflect any linear accelerator used in clinical practice, and different parameters would be needed in clinical dose calculations.

The library includes functionalities used for reading patient geometry, setting up beam geometry and running optimisation. IPOPT, an open source optimiser relying on

the interior point method for solving convex optimisation problems with constraints, is also included. Neither fluence optimisation nor DAO are generally convex problems, but the two step optimisation process and multiple beam directions are assumed to provide a local solution adequately close to the global optimum.

While the DL model used for dose prediction was trained on dose distributions produced by a VMAT optimiser, MatRad does not provide a VMAT optimisation framework. Instead, IMRT with 11 fixed beams of equidistant angles was used for each dataset and with each optimisation method. Optimised fluence maps were sequenced into static MLC segments and the resulting leaf positions further optimised as explained in Sections 3.1.2 and 3.1.3.

5 Experimental results

For the experimental results, a dose was optimised for each patient case using each optimisation method, defined in Section 3.2. The quality of each optimised dose was measured using a set of metrics described in the following section. Each metric is visualised as a deviation in percentage to the corresponding metric of the baseline predicted dose. As such, the aim of the visualisation is to demonstrate the ability of each optimisation method to provide equivalent or better dose quality than the baseline dose and to compare the performance of the optimisation methods.

5.1 Metrics

5.1.1 Homogeneity index

Each patient case has a target structure around the tumor and a prescribed dose level for the tumor. Ideally, a treatment plan would achieve a highly uniform dose on the whole target structure with small deviations. The deviation from homogeneity of the target dose is measured with the homogeneity index.

Let D_{mean} be the mean dose received by the target. In addition let, $D_{0.02}$ be the 98% quantile of the dose, that is, the dose level which 2% of the target exceeds and similarly $D_{0.98}$ the dose which 98% of the dose exceeds. The homogeneity index H is calculated as

$$H = \frac{D_{0.02} - D_{0.98}}{D_{mean}}.$$

Ideally, the difference between $D_{0.02}$ and $D_{0.98}$ is small and H is close to zero. In practice, however, the homogeneity index tends to be closer to 0.1 for most of the patient cases and optimisation approaches.

5.1.2 Conformity index

As mentioned in Section 3.2.1, high doses can leak around the target and cause hot spots in normal tissue. The conformity indices measure the extent to which doses above a certain threshold are concentrated on the target. Let D be the prescribed dose for the target and $k < 1$. In addition, let V_{target} be the volume of the target structure, $V_{k,target}$ the volume of the target with dose exceeding kD and $V_{k,body}$ the volume of the whole body with dose exceeding kD. The conformity index C_k is calculated as

$$C_k = \frac{V_{k,target}^2}{V_{target} V_{k,body}}.$$

The higher the proportion of the target receiving at least the reference dose and the smaller the volume outside the target receiving the reference dose, the closer to 1 the conformity index gets. Depending on the reference value of k chosen, good values for C_k can vary from 0.3 to 0.9. For the metrics in this thesis, values of $k = 0.95$ and $k = 0.5$ were chosen.

5.1.3 Organ metrics

For each organ, the mean dose and the 99th quantile dose is reported as the maximum dose. These are both important metrics for assessing the potential damage caused to organs by radiation.

For cases with highly variable locality and thereby different OARs, the deviation metrics for each organ are averaged. This means that for such cases the average deviation of all mean dose metrics from the baseline and similarly, the average deviation of all maximum dose metrics from the baseline are shown. Such cases are head and neck, lung and bone cases.

For the pelvis and prostate cases, the same set of organs were used in optimisation so each of the organ metrics can be reported separately. In these cases, the deviations from baseline were averaged separately for each organ across all the datasets in the corresponding category.

5.2 Discussion

The results, shown in Figures 8 - 12, feature metrics explained in the previous section. "Hi" refers to the homogeneity index as explained in Section 5.1.1 and "Ci95" and "Ci50" refer to conformity indices C_{95} and C_{50}, respectively. For bone, head and neck and lung cases, the deviations of mean and maximum doses from baseline are labeled with "Means" and "Maxima", respectively. For pelvis and prostate cases, the deviation of mean and max doses for each organ were averaged across the cases as explained in Section 5.1.3. Similarly to the organ metrics, the deviations of homogeneity and conformity indices for each category were averaged across all cases.

All the relative deviations from the baseline were averaged across the cases from each category, which are explained in Section 4.1. In the plots, these metric values are additionally scaled between -100% and 100% such that 0% is the baseline metric value and either -100% or 100% is the largest deviation of any optimisation method from the baseline.

The full voxel mimicking and labels voxel mimicking, also referred to as partial voxel mimicking in Section 3.2, are pure voxel mimicking methods. For these methods the quality deviation should optimally be close to zero or positive, reflecting the fact that these methods attempt to mimic the baseline dose but do not penalise dose values below the baseline in normal tissue. For the most part, partial voxel mimicking dominates full voxel mimicking except for the homogeneity index. Partial voxel mimicking places a relatively greater importance on the OARs through the assignment of optimisation weights for OARs, explaining why the OAR metrics are better. For the same reason, the PTV is assigned relatively lower significance, causing homogeneity indices to be worse. Nevertheless, both methods fail to produce good dose distributions.

The hybrid and conventional approaches are not pure voxel mimicking methods. Nevertheless, their ideal performance would show balanced quality deviation on the metrics. However, both hybrid approaches produced generally worse metrics than the baseline does, except for the lung and bone cases and to some extent the head and neck cases. Being only three datasets in total, some of the lung and bone cases could be outliers benefiting from an IMRT setup more than from VMAT. It could also be the case that the predicted dose is not optimal in these cases.

Out of all the methods, the conventional one seems to perform best for most cases and is the only one producing consistently better metrics for the head and neck cases than the baseline dose. However, it does not clearly dominate the other methods, as is obvious from the pelvis and prostate cases.

The results indicate that no optimisation method proved to be consistently of at least similar quality to the baseline predicted dose or dominate the other methods for all cases. However, dose optimisation is a multi-objective problem where each OAR and the PTV are given weights for optimisation with no guarantee that the weights are optimally chosen. This affects especially the conventional optimisation approach, whereas in the dose mimicking approaches no special consideration for weight selection needs to be given assuming the dose distribution to mimic is reachable with the optimiser at hand. It could be argued that with a different selection of weights the conventional approach could produce better results. The main issues are the poor homogeneity index and increased dose to certain organs in pelvis and prostate cases.

Figure 8: Aggregated metrics for bone cases

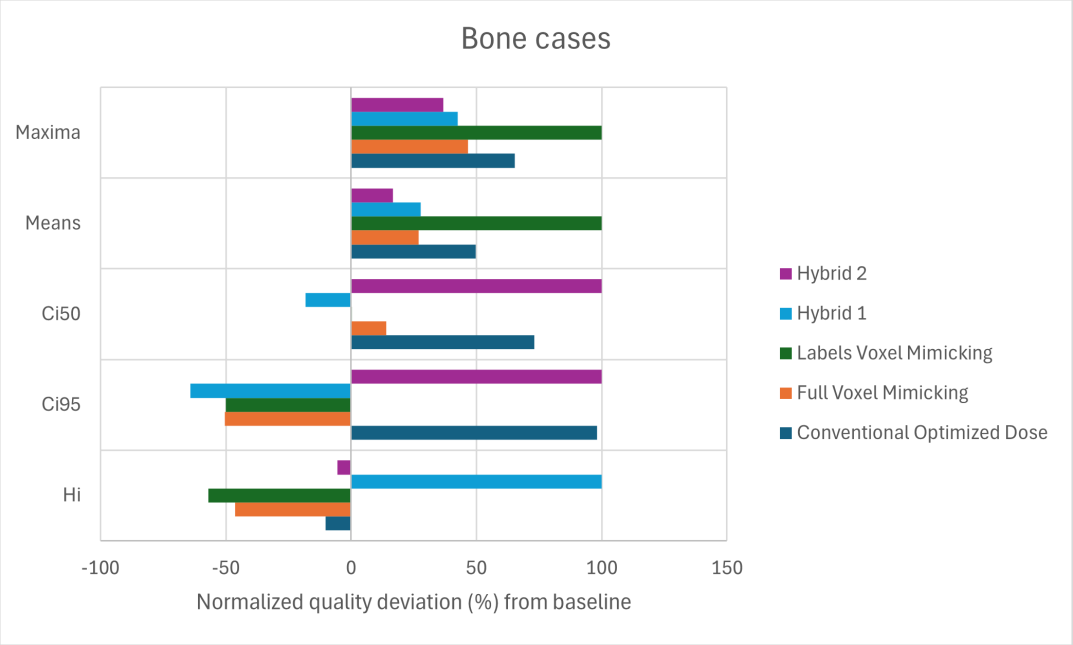

Figure 9: Aggregated metrics for head and neck cases

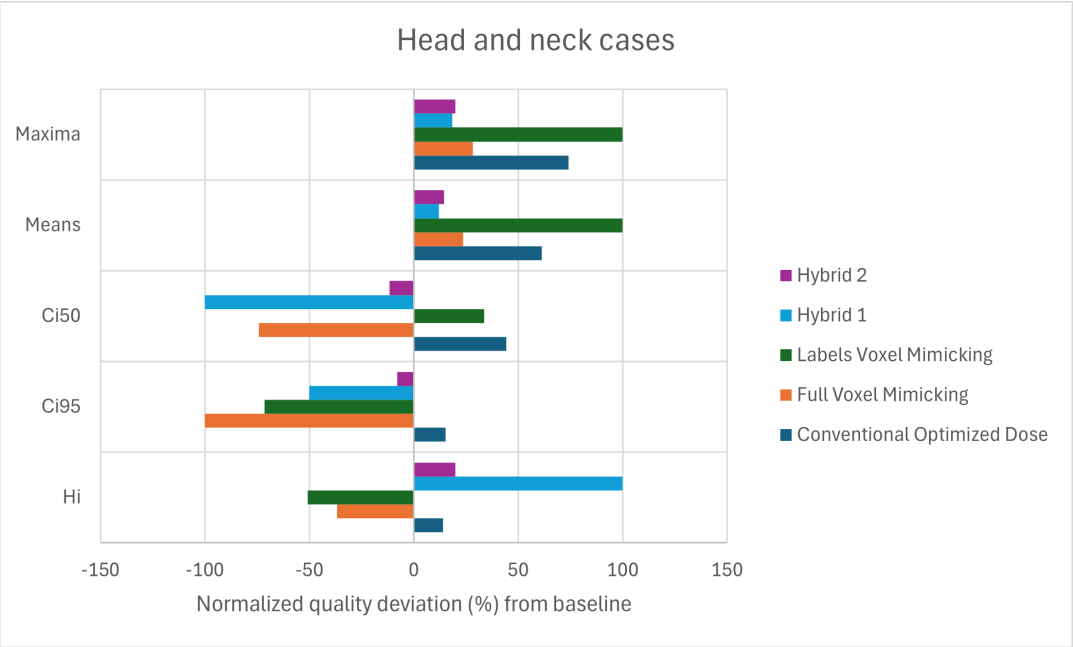

Figure 10: Metrics for the lung case

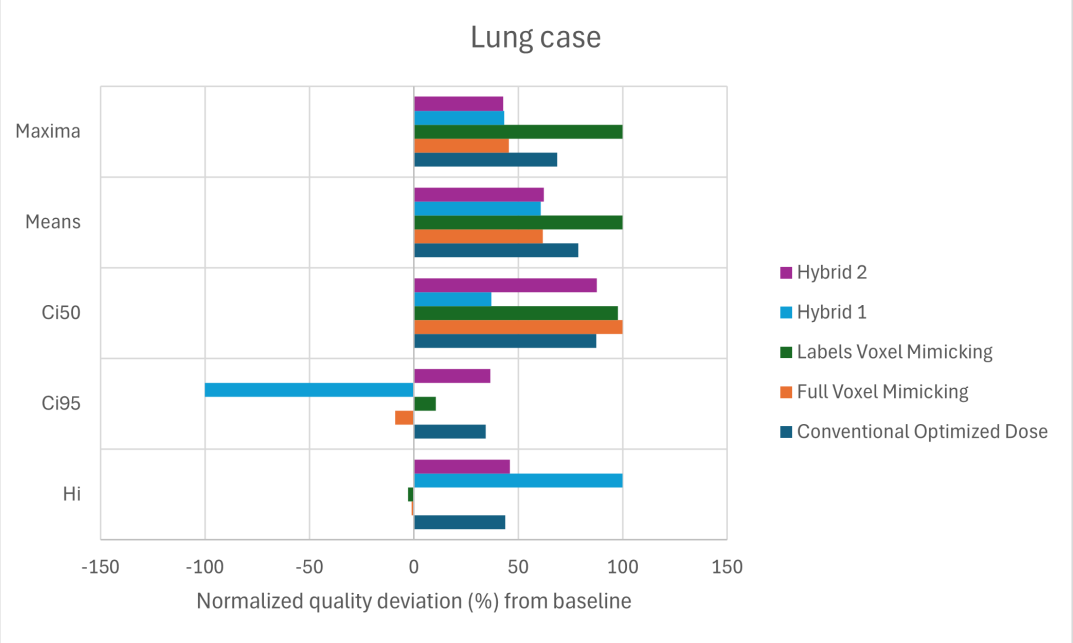

The failure of the voxel mimicking approaches to generate doses of similar quality to the baseline can be attributed to their inability to mimic the baseline dose: dose comparisons to the baselines reveal that the resulting dose distributions differ significantly from the baselines. There is nothing unexpected about this discovery - the baseline doses are predicted by a deep learning model using VMAT training data, with

no guarantees of achievability by an IMRT optimiser. The conventional optimisation objectives, however, only guide the optimiser to pursue a similar quality for the PTV and the organs to the baseline. These objectives are on a structure level, allowing much more variability in the final dose distribution than the voxel mimicking approaches. Hence, they are more agnostic to the specific optimisation problem definition or leaf sequencing algorithm used.

Figure 11: Aggregated metrics for pelvis cases

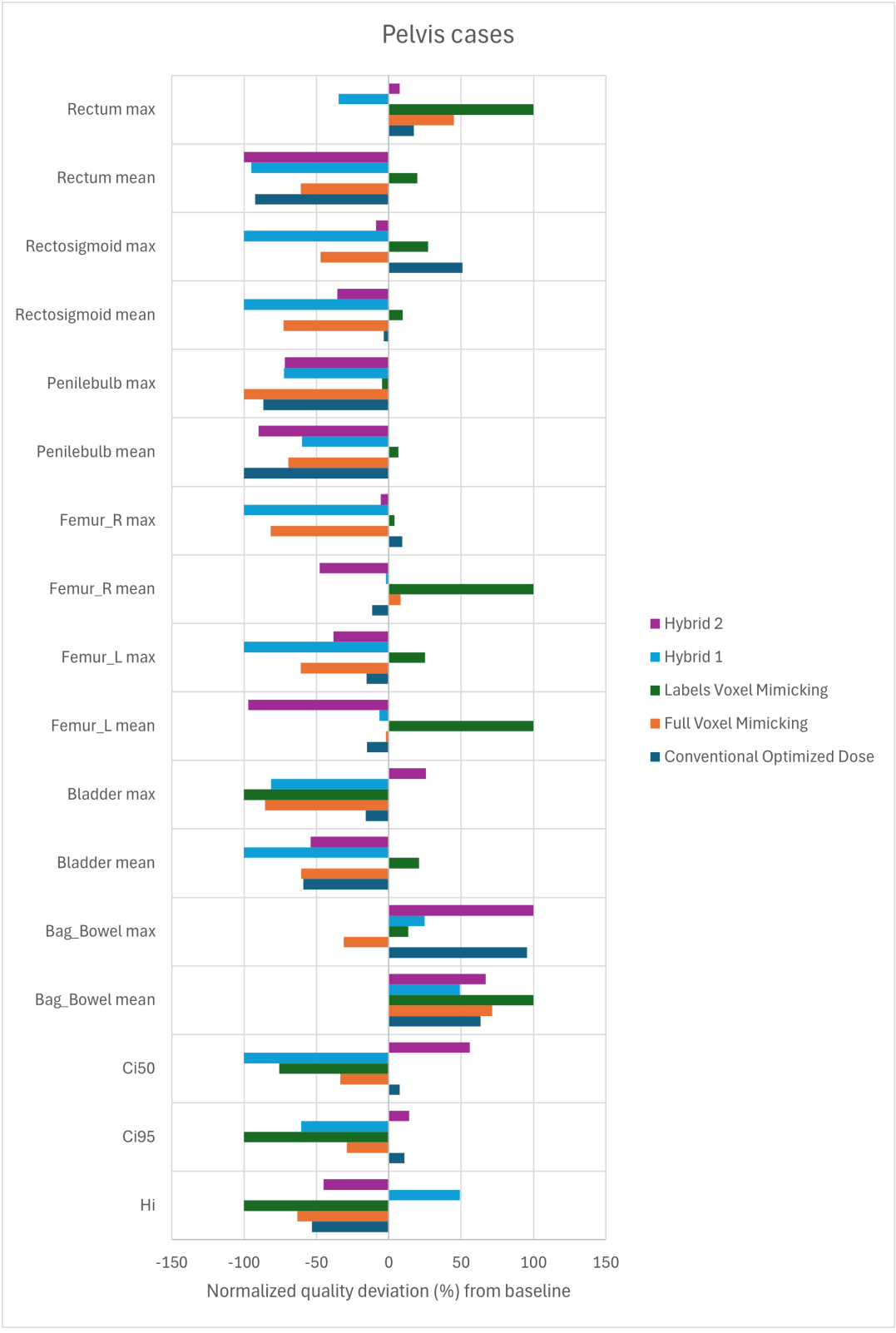

Figure 12: Aggregated metrics for prostate cases

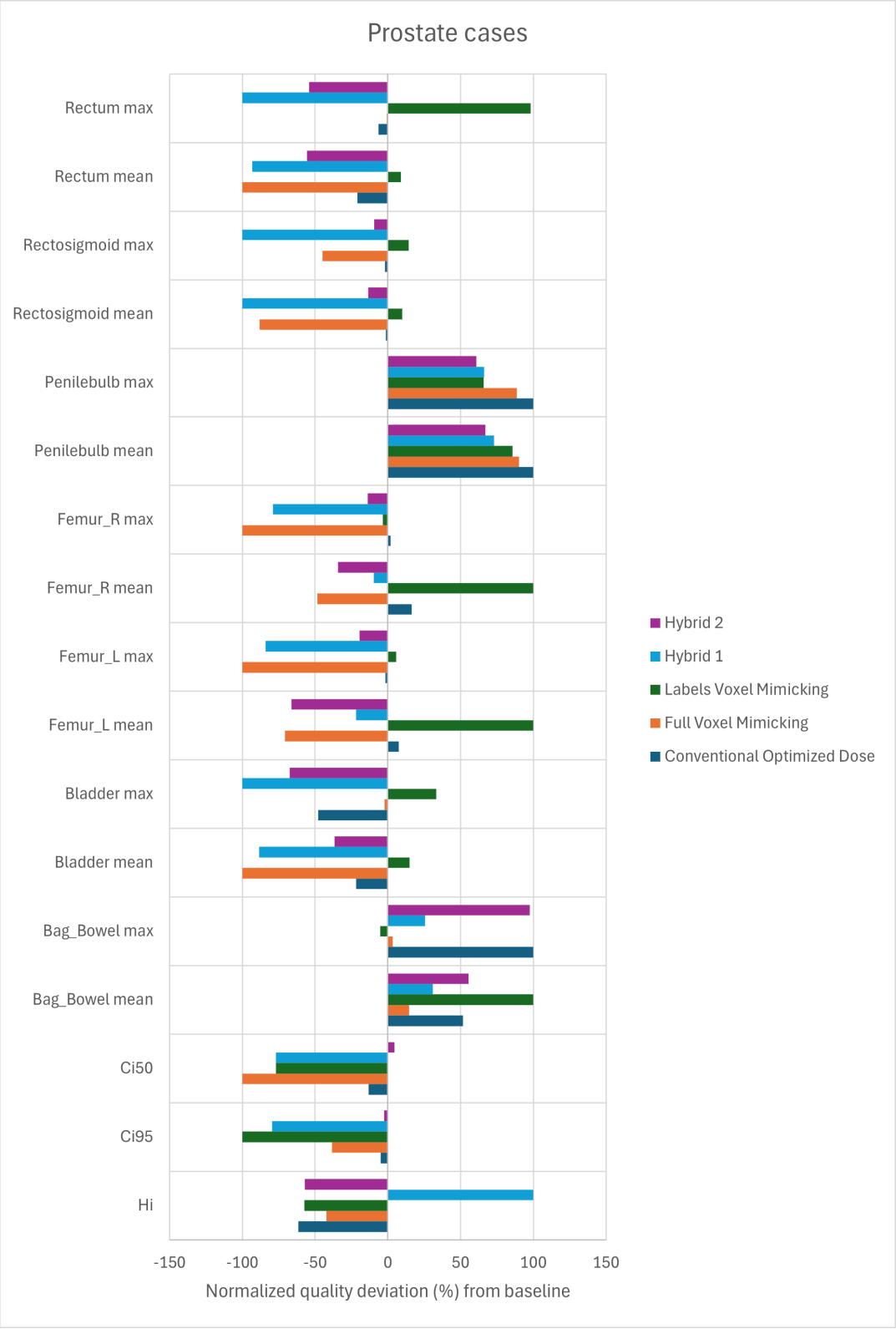

6 Conclusion

The aim of the thesis was to use MVision's dose prediction model for setting up optimisation objectives automatically and to evaluate the best optimisation approach for matching predicted dose quality with MatRad.

Dose mimicking, attempting to guide the optimiser towards the same dose as the predicted dose, produced poor results. Accuracy concerns of MatRad's pencil beam dose calculation in addition to differences between dose distributions produced by VMAT and IMRT treament plans are hypothesised to be the reason for the inability of these methods to mimic the predicted dose.

Using structure based objectives derived from DVH metrics of the predicted dose produced consistently at least equally good metrics as the other methods for bone, lung and head and neck cases. For the prostate and pelvis cases, no method clearly dominated others. However, visualisation of the results attest that the structure based objectives perform best, although not consistently able to match the dose quality of the predicted dose. This approach does not suffer from the unattainability of the predicted dose to the same extent as the dose mimicking approaches, as structure based optimisation objectives leave more room for variance inside structures without compromising dose quality. In light of this observation, better performance does not come as a surprise.

The thesis successfully demonstrates that using structure based objectives derived from a predicted dose distribution is a feasible approach with MVision's dose prediction model. The concept could be developed further into a fully automatised treatment planning process, in which a practitioner submits patient images with the prescribed dose into a system, receiving a clinically acceptable treatment plan without having to optimise the plan themselves.

However, the results also call for future research for both the structure based objectives and dose mimicking with a more standardised dose optimisation framework. Ideally, the dose prediction model should be trained with doses optimised with the same VMAT optimiser and the experiments of this thesis should be repeated with that same optimiser. Without these further developments, consistently adequate treatment plans can hardly be realised with a fully automatic optimisation process.

References

[1] Zaigham Abbas and Sakina Rehman. An overview of cancer treatment modalities. In Hafiz Naveed Shahzad, editor, *Neoplasm*, chapter 6. IntechOpen, Rijeka, 2018.

[2] Anders Ahnesjö and Maria Mania Aspradakis. Dose calculations for external photon beams in radiotherapy. *Physics in Medicine & Biology*, 44(11):R99, 1999.

[3] Mark R Arnfield, Christine Hartmann Siantar, Jeffrey Siebers, Pamela Garmon, Larry Cox, and Radhe Mohan. The impact of electron transport on the accuracy of computed dose. *Medical physics*, 27(6):1266–1274, 2000.

[4] Thomas Bortfeld. Imrt: a review and preview. *Physics in Medicine & Biology*, 51(13):R363, 2006.

[5] Thomas Bortfeld, Wolfgang Schlegel, and Bernhard Rhein. Decomposition of pencil beam kernels for fast dose calculations in three-dimensional treatment planning. *Medical physics*, 20(2):311–318, 1993.

[6] Anders Brahme, J-E Roos, and Ingemar Lax. Solution of an integral equation encountered in rotation therapy. *Physics in Medicine & Biology*, 27(10):1221, 1982.

[7] Karl Bzdusek, Henrik Friberger, Kjell Eriksson, Björn Hårdemark, David Robinson, and Michael Kaus. Development and evaluation of an efficient approach to volumetric arc therapy planning. *Medical physics*, 36(6Part1):2328–2339, 2009.

[8] David S Chang, Foster D Lasley, Indra J Das, Marc S Mendonca, Joseph R Dynlacht, et al. Basic radiotherapy physics and biology. Technical report, Springer, 2014.

[9] AAPM Radiation Therapy Committee, Arthur Boyer, et al. *Basic applications of multileaf collimators*. American Association of Physicists in Medicine Alexandria, VA, 2001.

[10] Daniel F Craft, Peter Balter, Wendy Woodward, Stephen F Kry, Mohammad Salehpour, Rachel Ger, Mary Peters, Garrett Baltz, Erik Traneus, and Rebecca M Howell. Design, fabrication, and validation of patient-specific electron tissue compensators for postmastectomy radiation therapy. *Physics and imaging in radiation oncology*, 8:38–43, 2018.

[11] Bahman Emami. Tolerance of normal tissue to therapeutic radiation. *Reports of radiotherapy and Oncology*, 1(1):123–7, 2013.

[12] Benedick A Fraass. The development of conformal radiation therapy. *Medical physics*, 22(11):1911–1921, 1995.

[13] Paolo Francescon, Carlo Cavedon, Sonia Reccanello, and Stefania Cora. Photon dose calculation of a three-dimensional treatment planning system compared to the monte carlo code beam. *Medical physics*, 27(7):1579–1587, 2000.

[14] Serena Gianfaldoni, Roberto Gianfaldoni, Uwe Wollina, Jacopo Lotti, Georgi Tchernev, and Torello Lotti. An overview on radiotherapy: from its history to its current applications in dermatology. *Open access Macedonian journal of medical sciences*, 5(4):521, 2017.

[15] V Grégoire and TR Mackie. State of the art on dose prescription, reporting and recording in intensity-modulated radiation therapy (icru report no. 83). *Cancer/Radiothérapie*, 15(6-7):555–559, 2011.

[16] Bjorn Hardemark, A Liander, H Rehbinder, and J Löf. Direct machine parameter optimization with raymachine in pinnacle. *Ray-Search White Paper*, 2003.

[17] Victor Hernandez, Christian Rønn Hansen, Lamberto Widesott, Anna Bäck, Richard Canters, Marco Fusella, Julia Götstedt, Diego Jurado-Bruggeman, Nobutaka Mukumoto, Laura Patricia Kaplan, et al. What is plan quality in radiotherapy? the importance of evaluating dose metrics, complexity, and robustness of treatment plans. *Radiotherapy and Oncology*, 153:26–33, 2020.

[18] Elham Hosseinzadeh, Nooshin Banaee, and Hassan Ali Nedaie. Cancer and treatment modalities. *Current Cancer Therapy Reviews*, 13(1):17–27, 2017.

[19] Noriyuki Kadoya, Yuto Kimura, Ryota Tozuka, Shohei Tanaka, Kazuhiro Arai, Yoshiyuki Katsuta, Hidetoshi Shimizu, Yuto Sugai, Takaya Yamamoto, Rei Umezawa, et al. Evaluation of deep learning-based deliverable vmat plan generated by prototype software for automated planning for prostate cancer patients. *Journal of Radiation Research*, 64(5):842–849, 2023.

[20] PJ Keall, JV Siebers, M Arnfield, JO Kim, and R Mohan. Monte carlo dose calculations for dynamic imrt treatments. *Physics in Medicine & Biology*, 46(4):929, 2001.

[21] U Kohl. Stellvorrichtung für röntgenröhren (device for x-ray tubes). *DRP*, 192:571, 1906.

[22] W Laub, M Alber, M Birkner, and F Nüsslin. Monte carlo dose computation for imrt optimization. *Physics in Medicine & Biology*, 45(7):1741, 2000.

[23] Lanchun Lu. Dose calculation algorithms in external beam photon radiation therapy. *International Journal of Cancer Therapy and Oncology*, 1(2), 2014.

[24] Colin D. Mathers, Ties Boerma, and Doris Ma Fat. Global and regional causes of death. *British Medical Bulletin*, 92(1):7–32, 09 2009.

[25] Chris McIntosh, Mattea Welch, Andrea McNiven, David A Jaffray, and Thomas G Purdie. Fully automated treatment planning for head and neck radiotherapy using a voxel-based dose prediction and dose mimicking method. *Physics in Medicine & Biology*, 62(15):5926, 2017.

[26] Peter Metcalfe, Alison Chapman, Anthony Arnold, Belinda Arnold, Puangpeng Tangboonduangjit, Anne Capp, and Chris Fox. Intensity-modulated radiation therapy: Not a dry eye in the house. *Australasian radiology*, 48(1):35–44, 2004.

[27] Brandon T Nguyen, Colin Hornby, Tomas Kron, Jim Cramb, Aldo Rolfo, Daniel Pham, Annette Haworth, Keen-Hun Tai, and Farshad Foroudi. Optimising the dosimetric quality and efficiency of post-prostatectomy radiotherapy: A planning study comparing the performance of volumetric-modulated arc therapy (vmat) with an optimised seven-field intensity-modulated radiotherapy (imrt) technique. *Journal of Medical Imaging and Radiation Oncology*, 56(2):211–219, 2012.

[28] Andrzej Niemierko. A generalized concept of equivalent uniform dose (eud). *Med Phys*, 26(6):1100, 1999.

[29] Andrzej Niemierko and Michael Goitein. Modeling of normal tissue response to radiation: the critical volume model. *International Journal of Radiation Oncology* Biology* Physics*, 25(1):135–145, 1993.

[30] Rany Nuraini and Rena Widita. Tumor control probability (tcp) and normal tissue complication probability (ntcp) with consideration of cell biological effect. In *Journal of Physics: Conference Series*, volume 1245, page 012092. IOP Publishing, 2019.

[31] Journal of the ICRU. Icru report 85, 2011.

[32] Karl Otto. Volumetric modulated arc therapy: Imrt in a single gantry arc. *Medical physics*, 35(1):310–317, 2008.

[33] Ervin B Podgorsak et al. *Radiation oncology physics.* IAEA Vienna, 2005.

[34] Cheng B Saw, R Alfredo C Siochi, Komanduri M Ayyangar, Weining Zhen, and Charles A Enke. Leaf sequencing techniques for mlc-based imrt. *Medical Dosimetry*, 26(2):199–204, 2001.

[35] Christian Scholz, Simeon Nill, and Uwe Oelfke. Comparison of imrt optimization based on a pencil beam and a superposition algorithm. *Medical Physics*, 30(7):1909–1913, 2003.

[36] David M Shepard, Matthew A Earl, X Allen Li, S Naqvi, and C Yu. Direct aperture optimization: a turnkey solution for step-and-shoot imrt. *Medical physics*, 29(6):1007–1018, 2002.

[37] DM Shepard, D Cao, MKN Afghan, and MA Earl. An arc-sequencing algorithm for intensity modulated arc therapy. *Medical physics*, 34(2):464–470, 2007.

[38] Jeffrey V Siebers, Marc Lauterbach, Shidong Tong, Qiuwen Wu, and Radhe Mohan. Reducing dose calculation time for accurate iterative imrt planning. *Medical physics*, 29(2):231–237, 2002.

[39] M Siggel, P Ziegenhein, S Nill, and U Oelfke. Boosting runtime-performance of photon pencil beam algorithms for radiotherapy treatment planning. *Physica Medica*, 28(4):273–280, 2012.

[40] Martin Siggel. *Concepts for the efficient Monte Carlo-based treatment plan optimization in radiotherapy*. PhD thesis, 2012.

[41] R Alfredo C Siochi. Minimizing static intensity modulation delivery time using an intensity solid paradigm. *International Journal of Radiation Oncology* Biology* Physics*, 43(3):671–680, 1999.

[42] RaySearch Laboratories AB SS. Biological optimization using the equivalent uniform dose (eud) in pinnacle3®, 2003.

[43] Shinji Takahashi. Conformation radiotherapy rotation techniques as applied to radiography and radiotherapy of cancer. *Acta Radiol. Suppl*, 1965.

[44] Hans-Peter Wieser, Eduardo Cisternas, Niklas Wahl, Silke Ulrich, Alexander Stadler, Henning Mescher, Lucas-Raphael Müller, Thomas Klinge, Hubert Gabrys, Lucas Burigo, et al. Development of the open-source dose calculation and optimization toolkit matrad. *Medical physics*, 44(6):2556–2568, 2017.

[45] Cedric X Yu. Intensity-modulated arc therapy with dynamic multileaf collimation: an alternative to tomotherapy. *Physics in Medicine & Biology*, 40(9):1435, 1995.